Structural and Morphological Studies of Isotactic Polypropylene Fibers during Heat/Draw Deformation by in-Situ Synchrotron SAXS/WAXD

Shaofeng Ran, Xinhua Zong, Dufei Fang, Benjamin S. Hsiao,* and Benjamin Chu*

Department of Chemistry, State University of New York at Stony Brook, Stony Brook, New York 11794-3400

Roger A. Phillips

Montell Polyolefins, R&D Center, 912 Appleton Road, Elkton, Maryland 21921

Received September 25, 2000

ABSTRACT: On-line studies of structural and morphological changes during the heating and drawing process of isotactic polypropylene (iPP) fiber were carried out using synchrotron small-angle X-ray scattering (SAXS) and wide-angle X-ray diffraction (WAXD) techniques. A unique image analysis method was used to deconvolute the two-dimensional (2D) WAXD patterns into quantitative fractions of crystal, mesomorphic, and amorphous phases. Results showed that the α-form crystals were quite defective in the initial iPP fibers and were converted into the mesomorphic modification by drawing at room temperature. Corresponding 2D SAXS patterns showed that there was no obvious long period (i.e., no lamellar structure) in the mesophase of the iPP fiber. We postulate that the constituents of the mesophase in iPP fibers include oriented bundles of helical chains with random helical hands and perhaps oriented chains with no helical structures; both have only partial packing ordering. The formation of the mesophase is through the destruction of the lamellar crystalline phase probably by pulling chains out from crystals. The α-form crystals were not converted into the mesophase by drawing at high temperatures. At higher temperatures, the α-form crystals became perfect and the crystallinity increased when the fiber was drawn. However, the draw ratio showed an inverse effect. The increase in draw ratio had a minimal effect on the crystallinity, but the transformation from the amorphous phase to the mesophase became dominant.

Introduction

There have been many studies on the structure, morphology, mechanical property, and their relationships in isotactic polypropylene (iPP). The commercial importance of this polymer is, of course, the main driving force for the mass efforts launched to investigate its solid-state organization.[1] However, there are still many more unresolved issues. For example, the nature of the mesophase and its relationships with the crystal phase in iPP fibers have not been completely developed, which is the focus of this work.

When crystallized from the melt or solution, iPP always adopts a 3_1 or 3_2 helical conformation in the crystalline structure. The helical chains can pack in different cell structures with specific helical hand registrations giving rise to different polymorphs of iPP, i.e., the α, β, and γ crystal forms, depending on the crystallization conditions.[2−5] In 1959, Natta et al.[6] pointed out the existence of the mesomorphic form of iPP when the sample was quenched from melt in ice water. The mesomorphic form has a degree of order intermediate between the amorphous phase and the crystalline phase. Natta et al. also concluded that the mesomorphic phase, in fact, is "smectic", containing bundles of parallel stretches of right- and left-handed 3-fold (3_1 and 3_2) helices. Since then, many comprehensive studies on the nature of the mesophase have been carried out. However, the experimental evidence for the "smectic" phase is still not conclusive.

Miller[7] suggested that the order existing in the mesophase could be of the type described by Hosemann[8] as "paracrystalline". This idea was reproposed by Zannetti et al[9,10] later. Wyckoff[11] found a certain degree of correlation between the adjacent helices in the mesophase, suggesting a short-range three-dimensional (3D) structure. Gailey and Ralston[12] pointed out that the partially ordered phase of iPP was composed of small hexagonal crystals. Gomez et al.[13] found that the packing of the 3-fold helices in the mesomorphic form was similar (at least at a very local scale) to that of the iPP chains in the β form by using high-resolution solid-state ^{13}C NMR. On the other hand, some researchers[14,15] assumed the mesomorphic form to be composed of microcrystals of the α form and suggested that the small crystal size broadened the X-ray diffraction peaks. Wunderlich and Grebowicz[16,17] proposed that the concept of conformationally disordered crystal was perhaps more appropriate to attribute to the mesomorphic form. This explanation was based on the hypothesis that the mesomorphic form of iPP might have a frozen-liquid-like structure, in which the 3-fold helices, as obtained from the melt, consisted of short chain segments with opposite signs of helical structure.

Corradini et al.[18,19] considered the various models corresponding to pseudohexagonal (as in the β form) and monoclinic (as in the α form) crystals, as well as several other disordered models possessing characters of both forms. They concluded that the mesomorphic form of iPP was not composed of small pseudohexagonal crystals but of much more disordered bundles of chains. Bruckner et al.[1] pointed out that the statistical structure of the mesomorphic iPP eliminated the possibility that the mesomorphic form might consist of small crystals of the α form or the β form. Results from deformation

* To whom all correspondence should be addressed. E-mail bhsiao@notes.cc.sunysb.edu or bchu@notes.cc.sunysb.edu.

10.1021/ma0016477 CCC: $20.00
Published on Web 03/10/2001

studies verified that the mesomorphic form was quite disordered in relation to the typical crystalline unit cell symmetries.[18,19] This disorder might be induced by the disruption of the existing crystallites through deformation forces.[20]

It is evident that although a great deal of work on the subject of the mesophase in iPP has been carried out, there are still some controversies in relation to the structure and the morphology of the mesophase, particularly in fibers during deformation. The objective of this study is to reexamine this subject with advanced X-ray scattering and diffraction techniques. To our knowledge, there are very few methods that can be used to separate the mesophase from the crystal phase. Martorana et al.[21] proposed a one-dimensional (1D) fitting procedure to determine the fractions of the three phases (crystal, mesomorphic, amorphous) in the quenched iPP samples. However, this method is not suitable to study the oriented samples such as fibers. In this study, a novel image analysis method has been introduced to analyze the 2D WAXD patterns of the quenched iPP fibers during heat and draw processes in order to obtain the quantitative information on the crystal, mesomorphic, and amorphous phases. The mesophase fraction extracted in this study represents the mass fraction of intermediate phase(s) between the amorphous phase and the ordered crystalline phase. This phase may be different from the "mesophase" mentioned above, which is often considered as the smectic phase, or even "mesomorphic" crystallite.[20] The mesomorphic content extracted in this work will include this contribution as well as the oriented amorphous chains, if any.

Experimental Section

The polypropylene fibers obtained from Montell USA were spun from a Hills model REM-3MP-25 spinning unit at a temperature of 216 °C and a take-up velocity of 1000 m/min. The resultant fiber was a 41-filament yarn with ~5 denier/filament. The spun fibers were quenched at air temperature of 13 °C. The resin was a commercial Ziegler−Natta resin (Montell PF-304) with M_w of $\sim 1.8 \times 10^5$ g/mol, M_w/M_n of ~3, melt flow rate index of 40 g/10 min, and zero shear viscosity of 6.25×10^3 P at 200 °C. The molecular weight and distribution were determined by gel permeation chromatography (GPC).

Synchrotron measurements were carried out at the X3A2 SUNY beam line, National Synchrotron Light Source (NSLS) at Brookhaven National Laboratory (BNL). The wavelength used was 1.54 Å. A three-pinhole collimator system[22,23] was used to reduce the beam size to 0.6 mm in diameter. The 2D WAXD patterns were recorded by a MAR CCD X-ray detector (MAR-USA) for quantitative image analysis. Separate simultaneous SAXS/WAXD patterns were also recorded using Fuji HR-V imaging plates (200 × 250 mm) which were then separately digitized by using a Fuji BAS 2000 IP imaging plate scanner.[24] The WAXD images from imaging plates were used to compare with the CCD images but were not analyzed. Only the SAXS images were analyzed for this study. The sample-to-detector distance for WAXD measurements with the CCD detector was 114.5 mm, which was calibrated by using an Al_2O_3 standard. The sample-to-detector distance for SAXS was 1138.0 mm. The collection time for both WAXD and SAXS was 2 min.

In this study, a continuous fiber draw apparatus was used (Figure 1). This industrial prototype draw apparatus was originally designed by A.D. Kennedy (DuPont), modified by us and constructed by Hills Inc. (W. Melbourne, Florida). The feeding speed was kept at 4 m/min during the experiment, while the drawing speed was continuously adjusted to achieve the desired draw ratio. The fiber was heated by two hot pins, located at 23 mm above the X-ray incident beam position on the fiber. The sample temperature was expected to be 5−15 deg lower than the temperature of the hot pins, depending on the contact time between the fiber and the hot pins. The temperature cited in this paper is the set temperature on the controller. The temperature of the hot pins was actually 3−10 deg higher than the set temperature. The fiber was kept running for about 10−15 min to make sure the draw ratio and the temperature were stable before taking X-ray images.

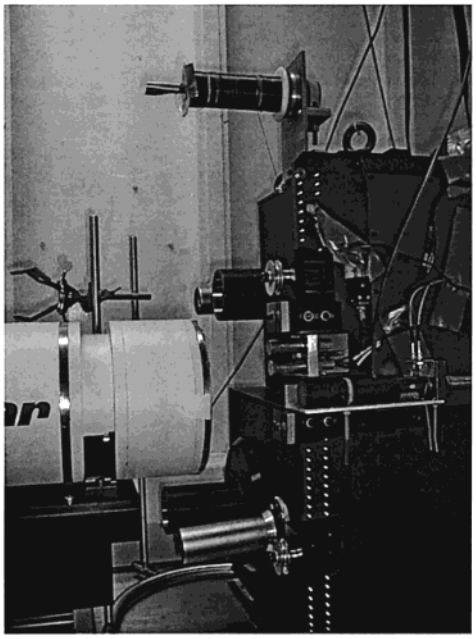

Figure 1. Picture of the continuous draw apparatus for on-line WAXD (or SAXS) measurement with MARCCD X-ray detector.

Data Analysis

1. Unit Cell Parameters. In relation to the crystal structure in real space, we can construct a reciprocal lattice unit cell in reciprocal space from the WAXD pattern. In terms of the unit cell, the general relationships between the dimensions of the real and reciprocal spaces are[25]

$$a^* = \frac{bc \sin \alpha}{V}$$

$$b^* = \frac{ca \sin \beta}{V}$$

$$c^* = \frac{ab \sin \gamma}{V} \qquad (1)$$

where a, b, c and α, β, γ are the unit cell dimensions and angles in real space, respectively; a^*, b^*, and c^* are the reciprocal lattice vectors directly determined from the 2D WAXD pattern. V is the volume of unit cell in real space. The unit cell parameters (a, b, c, α, β, γ) can be obtained from the positions of the reflections in WAXD patterns using the above equations. For multiple reflections superimposed on the same position, equal weight fractions are assigned for each reflection during the least-squares regression fitting, which has been demonstrated in a fiber draw study of nylon-66.[24]

2. Fractions of Crystal, Mesomorphic, and Amorphous Phases. For drawn fibers, the 2D WAXD pattern corrected for background and air scattering can be deconvoluted with a two-dimensional analytical method into two fractions: isotropic and anisotropic parts. The

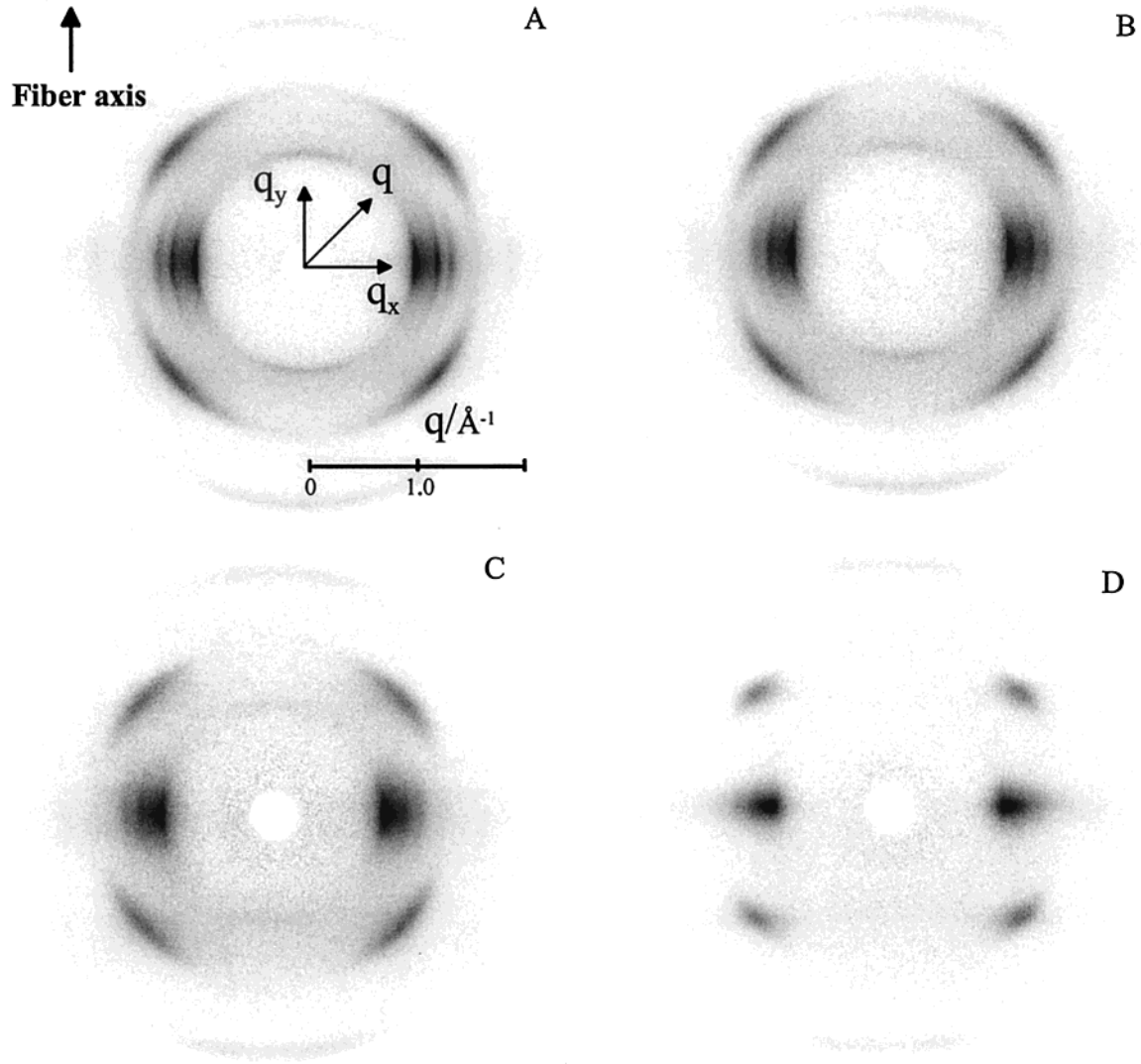

Figure 2. 2D WAXD patterns of iPP fiber with different draw ratios at room temperature. Draw ratio: A, 1.0; B, 1.5; C, 2.0; D, 2.5.

isotropic part includes the scattering from the amorphous phase and the Compton scattering from chemical structure which is usually small in a typical detection angular range and could be ignored. The isotropic fraction $A_{iso}(s)$ can be obtained using the following method. Starting from the center of the scattering pattern, a series of azimuthal scans can be obtained as a function of s ($s = 2\sin(\theta/2)/\lambda$, which is the scattering vector and θ is the scattering angle). The minimum intensity is determined from each azimuthal scan at a value of s. All of the minimum intensities at different values of s thus represent the envelope of the isotropic contribution. The problem of the low signals due to the detector response was corrected by an extrapolation routine.

The anisotropic fraction $A_{an}(s,\phi)$ then can be calculated from the following equation:

$$A_{an}(s,\phi) = A - A_{iso}(s) \qquad (2)$$

where A is the total scattering and ϕ represents the azimuthal scan angle. Note that $A_{iso}(s)$ is not a function of ϕ, but $A_{an}(s,\phi)$ is.

The anisotropic fraction can be further deconvoluted into mesomorphic and crystal fractions by using a two-dimensional peak fit method. Assuming that all reflections and scattering peaks (concentrated on the equator) from the crystal phase and the mesophase can be described by a series of two-dimensional functions such as the Gaussian function as following,[26] then we can use a 2D peak fit routine to fit the entire 2D WAXD patterns to separate the crystal and mesophase reflections.

$$f = h\exp\left(-\left(\frac{s_{x0} - s_x}{\omega_x}\right)^2 - \left(\frac{s_{y0} - s_y}{\omega_y}\right)^2\right) \qquad (3)$$

In eq 3, the subscript "0" represents the peak position, ω is the full width at half-maximum, h represents the height of the peak, s is the scattering vector, and s_x, s_y are the scattering vector values in the Cartesian coordinate of the reciprocal space ($s_x = 2\sin(\theta_x/2)/\lambda$). The principle of this 2D analysis method is identical to the one-dimensional peak deconvolution method to resolve the crystallinity in unoriented polymers.

Results and Discussion

1. Drawing at Room Temperature. Figure 2 illustrates the 2D WAXD patterns of iPP fiber with different draw ratios at room temperature. These WAXD patterns were corrected for beam fluctuations and air

Table 1. Unit Cell Parameters and Crystal Density of the Initial IPP Fiber without Drawing[a]

a (Å)	σ_a	b (Å)	σ_b	c (Å)	σ_c	D (g/cm^3)
6.62	0.04	21.13	0.10	6.77	0.06	0.90

[a] a, b, and c represent the unit cell parameters from a monoclinic unit cell; D represents the density of the unit cell. We assume the angles in the monoclinic cell remain about constant ($\alpha = \gamma = 90.0°$, $\beta = 99.2°$). σ is the standard deviation.

scattering. Figure 2A represents the pattern of the original fiber without drawing, which shows that the initial fiber is partially oriented. The three strong peaks located on the equator are the characteristic of the α-form crystal, which can be indexed as the (110), (040), and (130) reflections. Consistent with the literature, these three peaks are located at $2\theta = 14.3°$, 17.0°, and 18.7°.[27] However, it was noted that these three peaks were slightly broadened, which could be due to two reasons. One is that the formed crystals may be defective. The other is that there is the presence of the mesomophic form mixed with the α-crystal form in the original fiber. As the crystal density is often used to evaluate the perfection of the crystals, we have calculated the crystal density from the unit cell parameters refined from the WAXD pattern. The unit cell parameters and the crystal density are listed in Table 1. We found that the calculated crystal density was 0.90 g/cm^3 from the initial fiber, much lower than the ideal α-form crystal density (0.936 g/cm^3) and only slightly greater than the density of the mesophase (0.88 g/cm^3) measured by Natta et al.[6] This means that the formed crystals in the initial fiber are very defective.

With the increasing draw ratio, the azimuthal spread of the reflections became narrower, indicating that the crystal orientation increased with the draw ratio. It is interesting to see that the overlapping of the three α-form equatorial peaks also became more severe such that it is impossible to calculate the unit cell parameters for the fiber at larger draw ratios. At draw ratio equaling to 2.5, the three equatorial peaks completely disappeared, resulting in one broad peak on the equator. This broad peak and the weak but distinct four off-axis peaks (at the first layer line) (Figure 2D) are often regarded as the fingerprint of the mesomorphic form in iPP by WAXD.[28] From the 2D WAXD patterns in Figure 2, we conclude that the defective α-form crystals in the initial fiber are converted into the mesophase by drawing at room temperature. The four distinct peaks on the first layer line are due to the 3-fold helical chain structure, indicating that the mesophase maintains the 3-fold helical chain conformation, as has been confirmed by many earlier studies.[7,11,13,19−21] We hypothesize that the conversion process is through the chain pulling which eventually destroys the crystal structures. The packing of the helical hands (left and right) in the helical structures thus may be quite random in the mesophase.

A novel image analysis method has been used to deconvolute the fractions of crystal, mesomorphic, and amorphous phases from the 2D WAXD data. Considering that the mesophase represents the highly oriented fraction of the chains with poor intermolecular ordering when compared with the packing in crystals along the drawing direction and no specific registration of the helical hands, most of the scattered intensity contributed by the mesophase is expected to appear on the equator. The intensity of the scattering on the layer line due to the 3-fold helical structure is also present but relatively weak. In the 2D deconvolution procedure, we are only concerned about the intensity deconvolution on the equator for separation of the crystal phase and the mesophase. We assume that the ratio of the intensity fractions on the equator from the mesophase and the crystal phase is about the same as on the layer line. With this premise, we first select a region along the equatorial direction that contains the main crystal reflections (110, 040, and 130) and the broad mesophase scattering peak. Assuming that both the crystal reflection and the mesophase scattering can all be described by the 2D Gaussian functions (eq 3), the three crystal reflections ((110), (040), and (130)) and the mesophase background can be numerically deconvoluted. The mesophase scattering peak calculated in such a fashion is broad and more disordered than the crystal reflection peaks, which are narrow and with higher intensity. The mesophase fraction calculated by using this approach may include the ordered helical mesomorphic chains as well as the oriented chains with no helices. The latter needs to be elaborated here. Given the steric constraints of the methyl groups in iPP chains, an extended chain conformation is very unlikely. However, as the stereoregularity is not completely uniform in the chains, we envision that some segments of the chains containing stereo defects may be "stretched" but possess no helical conformation. In other words, a bundle of "wavy" chain segments with no helices may be presented. The mesophase value thus may overestimate the true mass fraction of the mesophase from the ordered helical chains. The procedure of this image analysis method is shown in Figure 3. The percentage of the residues in the 2D peak fit procedure was less than 2%. The corresponding 1D plot of the mesophase was similar to the one shown in the publication before.[20] The areas under the crystal reflection peaks and the mesophase scattering reflections calculated are thus used to estimate the fractions of the two different phases. We acknowledge that the accuracy of the mass fraction from each phase may not be precise, but the trend of the change during deformation should be informative.

Figure 4 shows the fractions of the crystal, mesomorphic, and amorphous phases as a function of draw ratio at room temperature using the above method. Some very interesting observations could be made in this figure. At low draw ratios (<1.5), the crystal fraction remained about constant, while the mesophase increased and the amorphous phase decreased slightly. Above a draw ratio of 1.5, the mesophase was seen to increase significantly. The corresponding crystal fraction and the amorphous phase all decreased, but a steeper decline was seen in the crystal phase. Our explanation is that the molecular mobility of the polymer chains is limited at room temperature, such that crystallization induced by drawing is not feasible. When the draw ratio is low, the energy provided by the stress is not sufficient to deform the crystal structure even though the crystals are defective. However, the chains in the amorphous phase could be oriented into the ordered phase, which constitutes part of the mesomorphic phase. When the draw ratio becomes sufficiently large, the energy provided by drawing can pull the helical chains out of the crystal and thus destroy the defective crystals. We envision that the stretched helical chains may aggregate into bundles with no specific arrangement of helical hands. With the addition of the "oriented chains with no helical hands" (possibly due to stereo defects) from

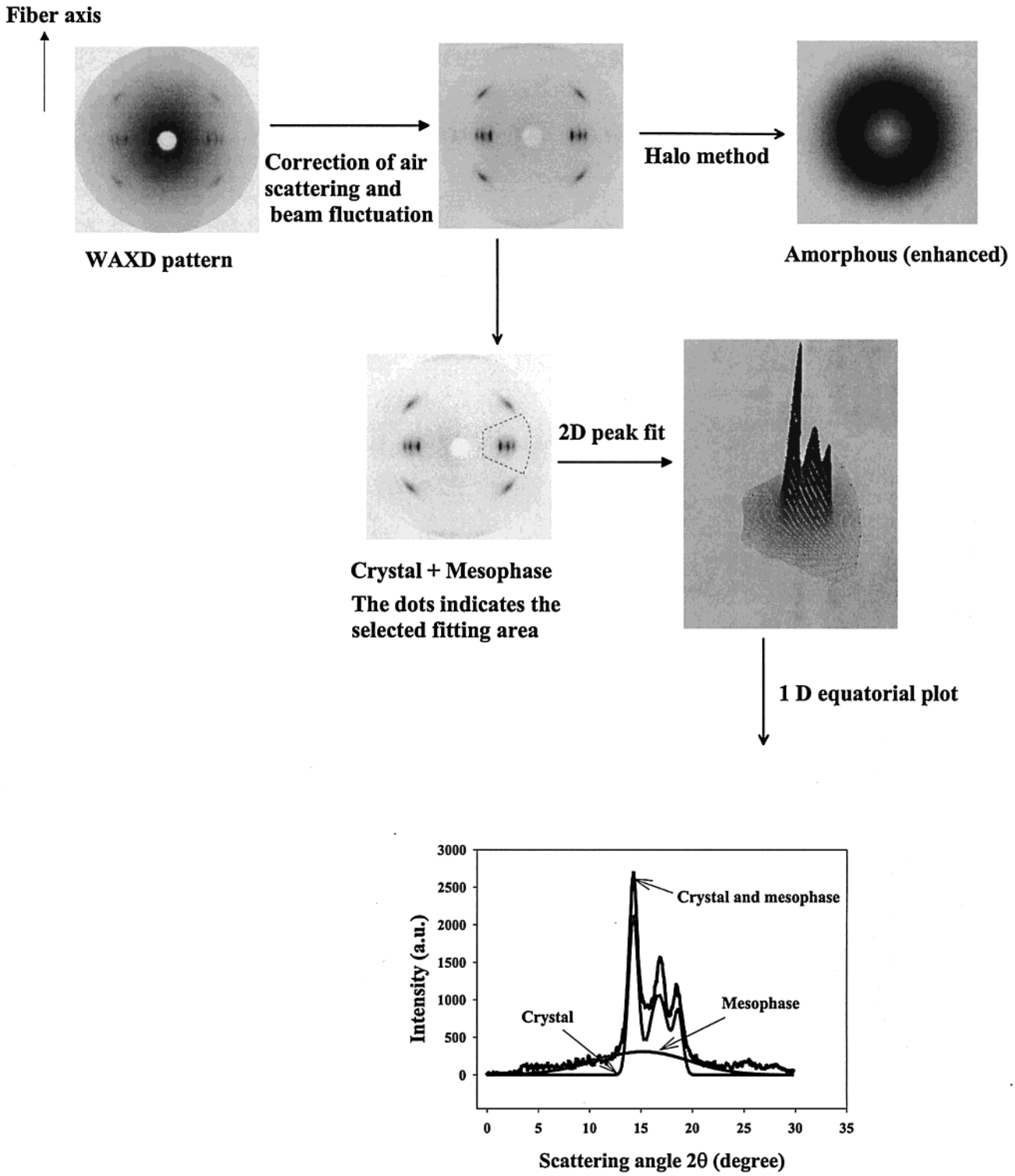

Figure 3. Procedures for deconvolution of crystal phase, mesophase, and amorphous phase from 2D WAXD patterns (iPP fiber at temperature of 100 °C and draw ratio of 2.0).

the pulling of the amorphous phase, the total fraction of the mesophase increased rapidly with the draw ratio at room temperature.

Figure 5 shows the corresponding 2D SAXS patterns of the iPP fiber at different draw ratios at room temperature. Figure 5A shows the pattern of the iPP fiber before drawing, exhibiting a two-bar pattern with the scattering maximum on the meridian. This indicates the presence of lamellar structure in the fiber. The intensity of the scattering peak was found to become weaker, and the two-bar pattern was smeared with the peak position shifting toward a low value (the long period becomes larger). These observations suggest the destruction of the lamellar structure. When the draw ratio reached 2.5, the two-bar pattern totally disappeared (Figure 5D), resulting in a strong streak pattern on the equator. This suggests that the lamellar structure is completely destroyed, forming a more disordered crystal structure but with highly oriented chains in a fibrillar morphology, in agreement with the results from

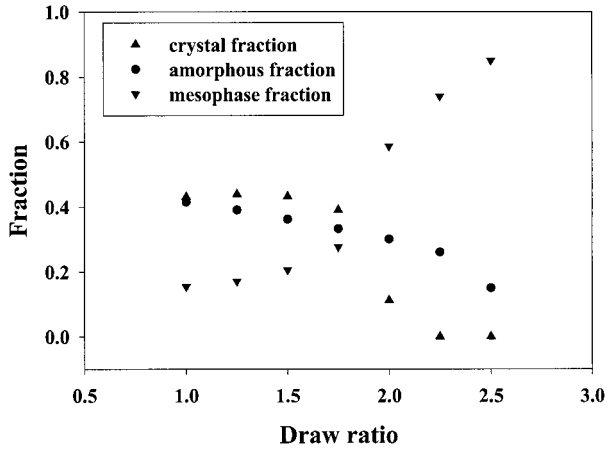

Figure 4. Fractions of crystal, mesomorphic, and amorphous phases as a function of draw ratio at room temperature.

WAXD. With the draw ratio larger than 2.0, the fraction of the mesophase approached 80% with almost little presence of the α-crystal phase (having three-dimensional ordering). The detailed morphological features for the mesomorphic phase have not yet been fully understood.[20] Early work of electron microscopy on the rapidly quenching samples noted "nodular" or "granular" structures on the order of 125 Å.[29,30] Grubb and Yoon claimed that the morphology of the mesophase resembled spherical "lumps" of diameter 100−350 Å.[31] However, the SAXS pattern of the mesophase in Figure 5D did not show any apparent "long period" in the fiber. The dominant mesophase in the drawn iPP fiber exhibits a SAXS pattern quite similar to the one from Kevlar fiber that is considered as having the fibril structure.[32] Thus, we postulate that the constituents of the mesophase in the drawn iPP fiber contain oriented bundles of polymer chains, in which the helical hands (left and right) are packing randomly or perhaps some with no helical hands. Thus, these molecular chains only have partial packing ordering. It is conceivable that the mesophase formed during the fiber drawing process has a different superstructure with the "nodular" or "granular" structure formed by quenching from the melt.

2. Drawing at Higher Temperatures. If we increase the draw temperature above 80 °C, the situation is completely different. Figure 6 shows the 2D WAXD patterns of the iPP fiber drawn at a ratio of 2.0 at different temperatures. It was found that the broad equatorial scattering from the mesophase (Figure 6A) was converted into three distinct α-form reflections (110, 040, 130). It is interesting to note that the layer line reflections also become much stronger after the draw process at a high temperature.

Figure 7 shows the changes of the mass fractions of the crystal, mesomorphic, and amorphous phases as a function of draw temperature at a fixed draw ratio of 2.0. It was found that the mesophase decreased rapidly with the draw temperature. The corresponding crystallinity was also found to increase, and the amorphous fraction was found to decrease with temperature. These

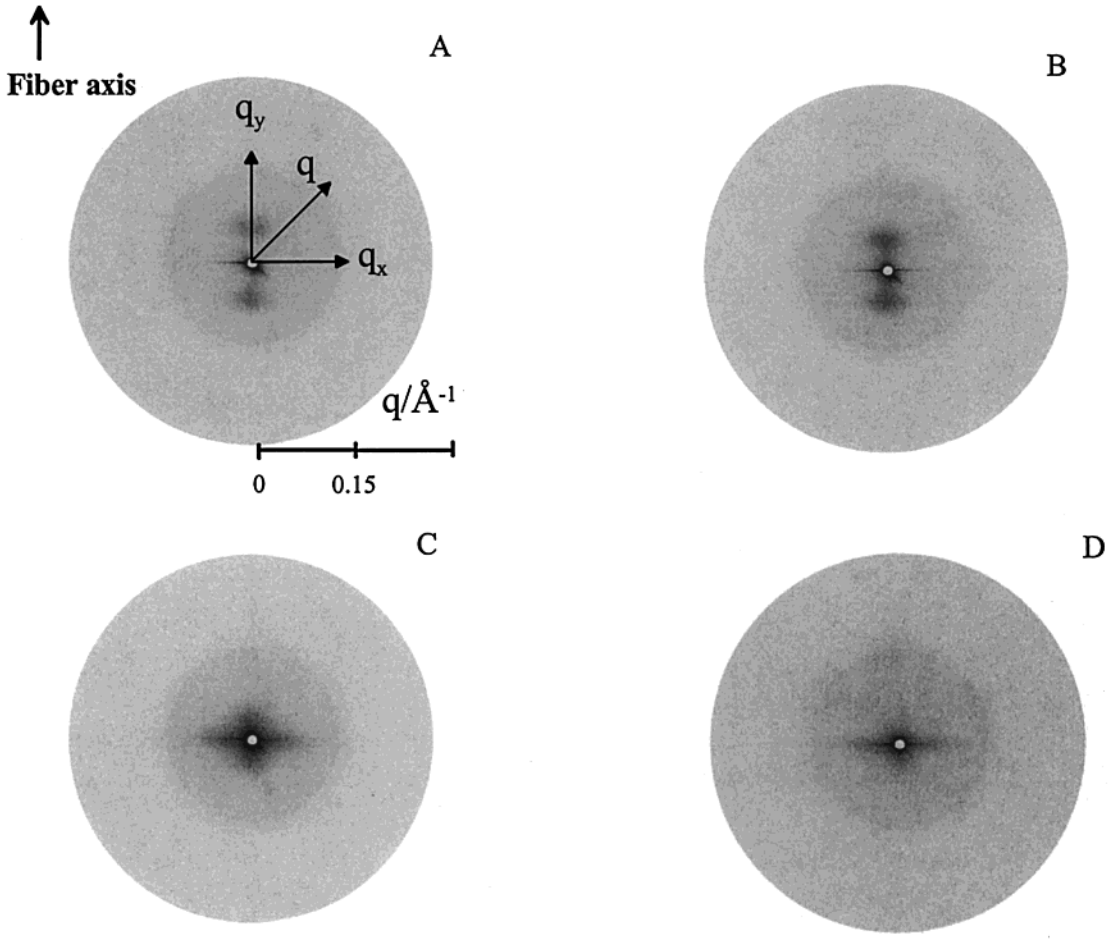

Figure 5. 2D SAXS patterns of iPP fiber with different draw ratios at room temperature. Draw ratio: A, 1.0; B, 1.5; C, 2.0; D, 2.5.

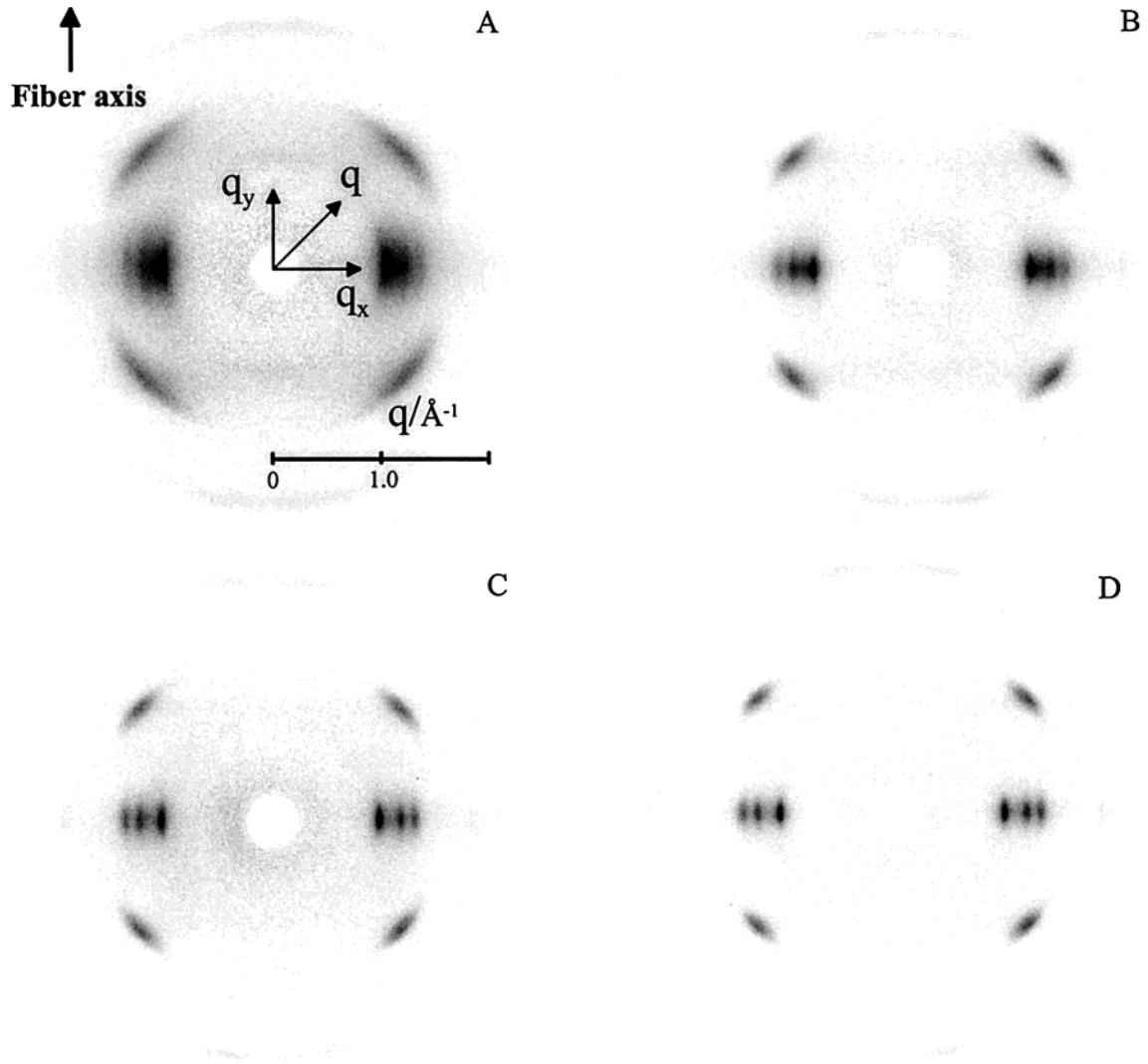

Figure 6. 2D WAXD patterns of iPP fiber with a draw ratio of 2.0 at different temperatures: A, room temperature; B, 80 °C; C, 100 °C; D, 110 °C.

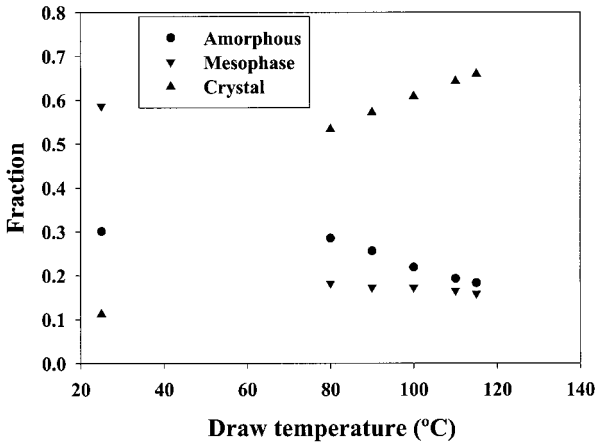

Figure 7. Mass fractions of crystal, mesomorphic, and amorphous phases as a function of draw temperature at a draw ratio of 2.0.

results indicate that when the draw temperature is higher, larger amounts of mesophase and amorphous phase can be converted into the crystal phase. Hsu et al.[30] investigated the morphological changes of iPP from the glassy state to the mesomorphic phase and then to the α-monoclinic crystal phase. They concluded that depending on the film thickness, the conversion to the α-form crystals became first detectable at 40 °C, which is somewhat consistent with our results. The difference in the transition temperature (80 °C in fibers in this study and 40 °C in the quenched unoriented films by Hsu) may be due to the different chain orientation in the samples. The higher chain orientation may hinder the chain reorganization process of getting the correct hands in the packing that is prerequisite for the crystallization of the α-monoclinic form. We have not investigated the temperature between 25 and 80 °C. The above results indicate that the mesomorphic phase is only metastable. We believe that an increase in temperature can provide the needed kinetic energy that facilitates the reorganization of the chains to form correct helical hands for crystallization as well as the perfection of the existing crystals in the fiber. As a result, the final crystallinity of the fiber drawn at high temperatures (>110 °C) approaches 70%.

The calculated unit cell parameters and the corresponding crystal density at different draw temperatures are listed in Table 2. It was found that the effect of draw temperature on the unit cell parameters was quite significant. The change in *a* was found to be very small and could almost be regarded as constant. However, both *b* and *c* showed a decrease with increasing draw

Table 2. Unit Cell Parameters and the Density of Isotactic Polypropylene Fibers at a Draw Ratio of 2.0 and Different Draw Temperatures[a]

draw temp (°C)	a (Å)	σ_a	b (Å)	σ_b	c (Å)	σ_c	D (g/cm^3)
80	6.58	0.02	21.30	0.07	6.74	0.04	0.901
90	6.62	0.03	21.21	0.08	6.70	0.05	0.903
100	6.61	0.03	21.11	0.07	6.68	0.04	0.912
110	6.61	0.03	20.96	0.08	6.65	0.05	0.922
115	6.61	0.03	20.97	0.07	6.65	0.04	0.922

[a] a, b, and c represent the unit cell parameters from a monoclinic unit cell; D represents the density of the unit cell. σ is the standard deviation.

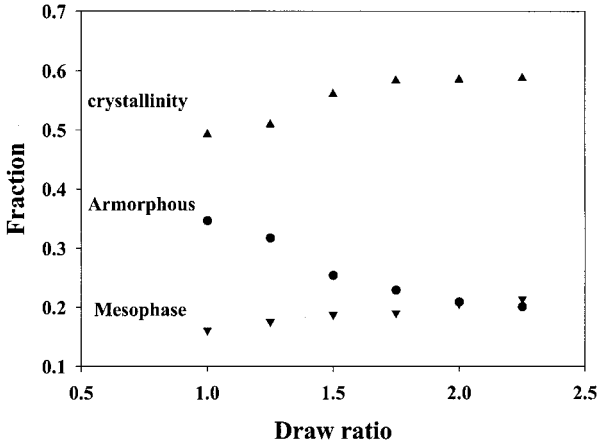

Figure 8. Variations of crystal, mesomorphic, and amorphous mass fractions as a function of draw ratio at a temperature of 100 °C.

temperature. The standard deviations were relatively small during refinement of the unit cell parameters, so the variation in the resultant cell dimensions could not be ignored (especially for b). The density of the crystal unit cell can be calculated from these parameters, which is also listed. It was found that the crystal density increased with the draw temperature, suggesting an increase in the crystal perfection with increasing temperature. This conclusion can also be made from the shape of the crystal reflections, which became much narrower and sharper with temperature.

Figure 8 shows the variation of the crystal, mesomorphic, and amorphous fractions as a function of draw ratio at a draw temperature of 100 °C. The results were also different from the drawing at room temperature. It was found that the mesophase was only a small fraction in the fiber and was increased slightly with draw ratio. Meanwhile, the crystallinity increased and the amorphous phase decreased with draw ratio. Both changes were greater than the change in the mesophase. These results suggest that at high temperatures drawing facilitates the conversion of the amorphous phase to both crystals and the mesomorphic phase. It is clear that drawing can promote the generation of the mesophase by pulling out the helical chains from the crystals. The high temperature apparently facilitates the intermolecular registration of the helical chains to form three-dimensionally ordered crystals. As a result, the crystallinity increases the most with draw ratio at high temperatures. On the other hand, at high draw ratios, the large restriction on the chains may retard the process of "sorting" the correct hands by reorganization of the chains, making crystallization more difficult to take place. This may be the reason why the crystallinity does not change at draw ratios larger than 1.75, as shown in Figure 8. From the results above, it is noted that the mesophase is quite metastable at high temperatures (such as 100 °C). So it is conceivable that the mesomorphic content in this situation is mainly composed of the oriented amorphous chains (perhaps with no helices). That is why the mesophase fraction is small at 100 °C.

Table 3. Unit Cell Parameters and Crystal Density of Isotactic Polypropylene Fibers at 100 °C and Different Draw Ratios

draw ratio	a (Å)	σ_a	b (Å)	σ_b	c (Å)	σ_c	D (g/cm^3)
1.00	6.66	0.02	21.07	0.06	6.66	0.04	0.909
1.25	6.63	0.03	21.09	0.07	6.69	0.04	0.909
1.50	6.63	0.02	21.08	0.06	6.68	0.02	0.910
1.75	6.62	0.02	21.05	0.06	6.69	0.04	0.912
2.00	6.61	0.03	21.11	0.07	6.68	0.04	0.912
2.25	6.61	0.03	21.12	0.07	6.68	0.04	0.911

[a] a, b, and c represent the unit cell parameters from a monoclinic unit cell; D represents the density of the unit cell. σ is the standard deviation.

Table 3 listed the results of the unit cell dimensions and the crystal density at 100 °C. Compared with Table 2, the unit cell dimensions and the crystal density remained about constant, indicating that the effect of draw ratio on the unit cell parameters at high temperatures is small. If there is any change, we find that the crystal density increases slightly with draw ratio at high temperatures.

Figure 9 shows 2D SAXS patterns of iPP fiber with draw ratio of 2.0 at different draw temperatures. It was found that the lamellar structure again prevailed when the draw temperature was increased to 80 °C. This is evident that the two-bar pattern became more apparent with increasing temperature.

The correlation function[33] and the interface distribution[34−37] function have been used to analyze the SAXS profile from isotropic systems to resolve the thicknesses of the constituent phases (crystal and amorphous) in the lamellar structure.[34] However, these functions are not easy to use directly for anisotropic systems, such as fibers. For example, if the fiber is only partially oriented, the meridionally sliced SAXS profile will have to be corrected by the Lorentz factor (i.e., the Iq^2 value to represent the integrated scattered intensity). If the fiber is completely oriented, the meridionally sliced SAXS profile becomes identical to the integrated scattered intensity, and the correlation and the interface distribution function can be directly calculated from the Fourier transformation of the sliced intensity. Since it is difficult for us to precisely determine the degree of orientation in the fibers and the validity of using the proper correction, we have opted not to rely on the correlation or the interface distribution functions to estimate the crystal and amorphous thickness. Some authors have used the product of the long period (L) and the bulk crystallinity (ϕ_c from WAXD) to represent the crystal thickness (l_c).[38−40] Then the amorphous thickness (l_a) would be

$$l_a = L - l_c \tag{4}$$

This method has an assumption that the resultant morphology consists of space-filled lamellar stacks. This is not true if there is a fraction of noncrystalline gap residing outside the lamellar stacks, especially in the sample of low crystallinity (<40%).[41] However, in this

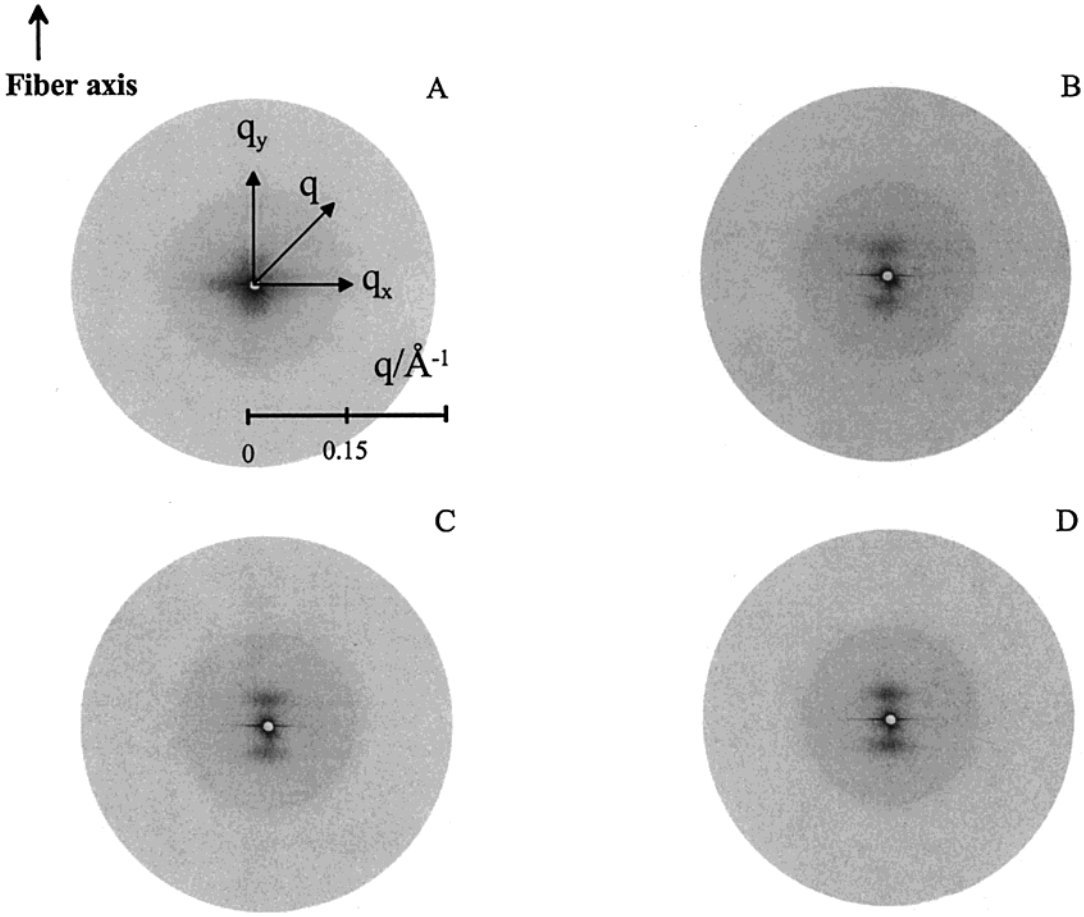

Figure 9. 2D SAXS patterns of iPP fiber with a draw ratio of 2.0 at different temperatures: A, room temperature; B, 80 °C; C, 100 °C; D, 110 °C.

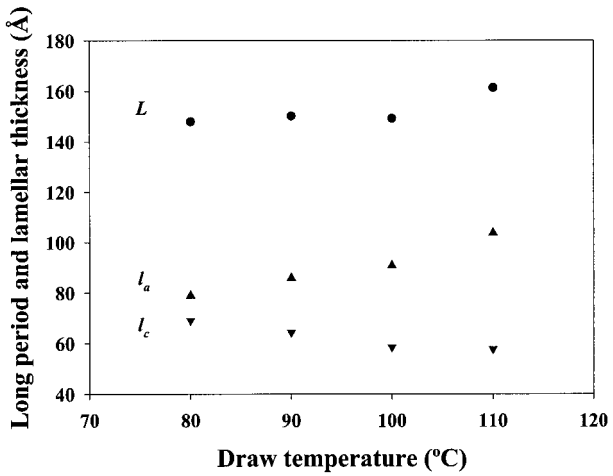

Figure 10. Changes of long period, crystal thickness, and amorphous layer thickness during iPP fiber drawing at a draw ratio of 2.0 and different temperatures.

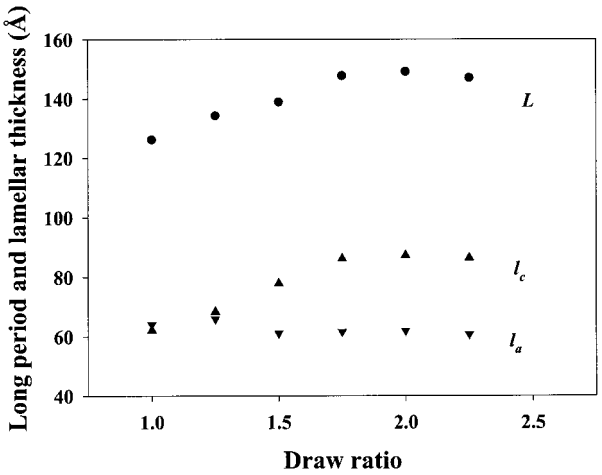

Figure 11. Changes of long period, crystal thickness, and amorphous layer thickness during iPP fiber drawing at a temperature of 100 °C and different draw ratios.

work, since the crystallinity of the fiber is larger than 50% at draw temperature higher than 80 °C, it is feasible to use this method to roughly estimate the crystal and amorphous thickness.

Figure 10 shows the long period, the crystal thickness, and the amorphous thickness calculated using the above method at draw ratio of 2.0 and different draw temperatures. In this calculation, we assume that there is only the two-phase structure (alternating crystal and amorphous phases) that gives rise to the scattering pattern, and the contribution of the mesophase is irrelevant. We believe this is a reasonable assumption, as the mass fraction of the mesophase is small (about 15%) at this stage. The exact location of the mesophase is not clear, but it is likely that the mesophase resides outside the lamellar stacks (in the superstructure of fibril) and does not contribute to the two-bar scattering patterns. (In Figure 9A, as we cannot identify the lamellar structure in the fibers, no calculation has been carried out.) In Figure 10, the long period was found to increase slowly with increasing draw temperature. Meanwhile, the crystal thickness increased rapidly, and the amorphous

thickness decreased, implying that more chains in the amorphous phase were crystallized with increasing draw temperature. This observation indicates that the recrystallization process perfects the existing lamellae and allows them to be thickened. The crystal perfection results are consistent with our earlier findings with WAXD.

Figure 11 shows the long period, the lamellar thickness at the draw temperature of 100 °C, and different draw ratios. The long period and the crystal thickness were found to increase before the draw ratio reached the value of 2.0. The corresponding amorphous thickness remained unchanged with draw ratio. This result indicates that drawing at high temperatures also perfects the crystals. The long period, the crystal, and amorphous thicknesses did not change when the draw ratio became larger than 2.0. Again, this is consistent with our earlier WAXD results that at high draw ratios the transition from the amorphous phase to the mesophase became dominant and thereby did not affect the overall lamellar structure.

Conclusions

On-line studies of structural and morphological development were carried out during the drawing of the isotactic polypropylene fibers by in-situ synchrotron SAXS/WAXD techniques. A novel image analysis method was used to deconvolute the quantitative information on the mass fractions of the crystalline, mesomorphic, and amorphous phases from the 2D WAXD patterns. Results indicated that defective α-form crystals were present in the initial iPP fibers. These α-form crystals were completely converted into the mesomorphic form at draw ratios above 2.5 at room temperature. The corresponding 2D SAXS pattern showed that there was no obvious lamellar structure in the mesophase of the iPP fibers. We speculate that the dominant constituent of the mesophase in iPP fibers may be oriented bundles of helical chains with random helical hands in addition to the oriented chains with no helical structures due to stereo defects, with both having only partial packing ordering, but no short-range three-dimensional orders. The α-form crystals were not converted to the mesophase at high draw temperatures. Under these conditions, the α-form crystals became more perfect, and the crystallinity also increased during drawing. At 100 °C, results showed that the amorphous phase was converted into both mesophase and crystal phase at low draw ratios. At high draw ratios, the transition from the amorphous phase to the mesophase became more dominating, may be because the crystallization at high draw ratios was more difficult since the restriction on the stretched chains became greater and thus made the chains more difficult to reconfigure into the correct helical hand registration that is necessary for crystallization.

Acknowledgment. The authors thank Mr. Richard Hilmer for his assistance in developing the image analysis software. B.C. and B.H. are grateful for the financial support of this work by a grant from the US Army Research Office (DAAD190010419). B.H. also acknowledges the financial support from the NSF Center for Advanced Engineering Fibers and Films at Clemson University.

References and Notes

(1) Bruckner, S.; Meille, S. V.; Petraccone, V.; Pirozzi, B. *Prog. Polym. Sci*. **1991**, *16*, 361.

(2) Caldas, V.; Brown, G. R.; Nohr, R. S.; MacDonald, J. G.; Raboin, L. E. *Polymer* **1994**, *35*, 899.

(3) Morris, D. R. *J. Macromol. Sci., Phys*. **1969**, *B3*, 53.

(4) Lotz, B.; Wittmann, J. C. *J. Polym. Sci., Polym. Phys. Ed*. **1986**, *24*, 1541.

(5) Lotz, B.; Graff, S.; Wittmann, J. C. *J. Polym. Sci., Polym. Phys. Ed*. **1986**, *24*, 2017.

(6) Natta, G.; Peraldo, M.; Corradini, P. *Rend. Accad. Naz. Lincei* **1959**, *26*, 14.

(7) Miller, R. L. *Polymer* **1960**, *1*, 135.

(8) Hosemann, R. *Acta Crystallogr*. **1951**, *4*, 520.

(9) Zannetti, R.; Celotti, G.; Fichera, A.; Francesconi, R. *Makromol. Chem*. **1969**, *128*, 137.

(10) Zannetti, R.; Celotti, G.; Armigliato, A. *Eur. Polym. J*. **1970**, *6*, 879.

(11) Wycoff, H. W. *J. Polym. Sci*. **1962**, *62*, 83.

(12) Gailey, J. A.; Ralston, P. H. *Plast. Eng. Trans*. **1964**, *4*, 29.

(13) Gomez, M. A.; Tanaka, H.; Tonelli, E. *Polymer* **1987**, *28*, 2227.

(14) Bodor, G.; Grell, M.; Kallo, A. *Faserforsch. Textil-Tech*. **1964**, *15*, 527.

(15) Farrow, G. *J. Appl. Polym. Sci*. **1965**, *9*, 1227.

(16) Wunderlich, B.; Grebowicz, J. *J. Adv. Polym, Sci*. **1984**, *60/61*, 1.

(17) Grebowicz, J.; Lau, J. F.; Wunderlich, B. *J. Polym. Sci., Polym. Symp*. **1984**, *71*, 19.

(18) Corradini, P.; Petraccone, V.; De Rosa, C.; Guerra, G. *Macromolecules* **1986**, *19*, 2699.

(19) Corradini, P.; De Rosa, C.; Guerra, G.; Petraccone, V. *Polym. Commun*. **1989**, *30*, 281.

(20) Phillips, R. A.; Wolkowicz, M. D. In *Polypropylene Handbook;* Moore, Jr., E. P., Ed.; Hanser Publishers: Munich, 1996; p 419.

(21) Martorana, A.; Piccarolo, S.; Scichilone, F. *Macromol. Chem. Phys*. **1997**, *198*, 597.

(22) Chu, B.; Harney, P. J.; Li, Y.; Linliu, K.; Yeh F.; Hsiao, B. S. *Rev. Sci. Instrum*. **1994**, *65*, 597.

(23) Hsiao, B.; Chu, B.; Fengji Yeh. *NSLS Newsletter* **1997**, July, 1−4.

(24) Hsiao, B. S.; Chu, B.; Harney, P.; Kennedy, A. D.; Leach, R. A. *J. Appl. Crystallogr*. **1997**, *30*, 1084.

(25) Alexander, L. E. *X-Ray Diffraction Methods in Polymer Science;* John Wiley & Sons: New York, 1969.

(26) Abramowitz, M.; Stegun, I. A. *Handbook of Mathematical Functions with Formulas, Graphs and Mathematical Tables;* Applied Mathematics Series 55; U.S. Department of Commerce, National Bureau of Standards: Washington, DC, 1964; p 1045.

(27) Huang, M.; Li, X.; Fang, B. *J. Appl. Polym. Sci*. **1995**, *56*, 1323.

(28) de Candia, F.; Iannelli, P.; Staulo, G.; Vittoria, V. *Colloid Polym. Sci*. **1988**, *266*, 608.

(29) Gezovich, D. M.; Geil, P. H. *Polym. Eng. Sci*. **1968**, *8*, 202.

(30) Hsu, C. C.; Geil, P. H.; Miyaji, H.; Asai, K. *J. Polym. Sci., Polym. Phys. Ed*. **1986**, *24*, 2379.

(31) Grubb, D. T.; Yoon, D. Y. *Polym. Commun*. **1986**, *27*, 84.

(32) Grubb, D. T.; Prasad, K.; Adams, W. *Polymer* **1991**, *32*, 1167.

(33) Vonk, C. G.; Kortleve, G. *Colloid Polym. Sci*. **1967**, *220*, 19.

(34) Ruland, W. *Colloid Polym. Sci*. **1977**, *255*, 417.

(35) Fiedel, H. W.; Wenig, W. *Colloid Polym. Sci*. **1989**, *267*, 389.

(36) Stribeck, M.; Ruland, W. *J. Appl. Crystallogr*. **1978**, *11*, 535.

(37) Wenig, W.; Scholler, T. *Prog. Colloid Polym. Sci*. **1985**, *71*, 113.

(38) Medellin-Rodriguez, F. J.; Phillips, P. J.; Lin, J. S. *Macromolecules* **1996**, *29*, 7491.

(39) Groeninchx, G.; Reynaers, H.; Berghmans, H.; Smets, G. *J. Polym. Sci., Polym. Phys*. **1980**, *18*, 1311.

(40) Medellin-Rodriguez, F. J.; Phillips, P. J.; Lin, J. S.; Campus, R. *J. Polym. Sci., Polym. Phys*. **1997**, *35*, 1757.

(41) Wang, Z. G.; Hsiao, B. S.; Fu, B. X.; Liu, L.; Yeh, F.; Sauer, B. B.; Chang, H.; Schultz, J. M. *Polymer* **2000**, *41*, 1791.

MA0016477